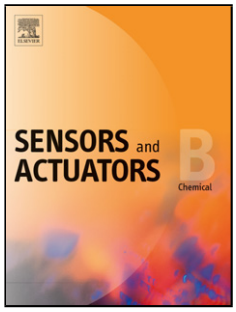

Title: Fine discrimination of volatile compounds by graphene-immobilized odorant-binding proteins

Authors: Caroline Kotlowski, Melanie Larisika, Patrick M. Guerin, Christoph Kleber, Thomas Kröber, Rosa Mastrogiacomo, Christoph Nowak, Paolo Pelosi, Stefan Schütz, Andreas Schwaighofer, Wolfgang Knoll

PII: S0925-4005(17)31995-0
DOI: https://doi.org/10.1016/j.snb.2017.10.093
Reference: SNB 23397

To appear in: *Sensors and Actuators B*

Received date: 18-5-2017
Revised date: 7-10-2017
Accepted date: 16-10-2017

Please cite this article as: Caroline Kotlowski, Melanie Larisika, Patrick M.Guerin, Christoph Kleber, Thomas Kröber, Rosa Mastrogiacomo, Christoph Nowak, Paolo Pelosi, Stefan Schütz, Andreas Schwaighofer, Wolfgang Knoll, Fine discrimination of volatile compounds by graphene-immobilized odorant-binding proteins, Sensors and Actuators B: Chemical https://doi.org/10.1016/j.snb.2017.10.093

Fine discrimination of volatile compounds by graphene-immobilized odorant-binding proteins

Caroline Kotlowski[a,b,‡], Melanie Larisika[a,b,‡], Patrick M. Guerin[c], Christoph Kleber[a], Thomas Kröber[c], Rosa Mastrogiacomo[d], Christoph Nowak[a,b], Paolo Pelosi[d], Stefan Schütz[e], Andreas Schwaighofer[f], Wolfgang Knoll[a,b,*]

[a)] Center for Electrochemical Surface Technology, 2700 Wiener Neustadt, Austria

[b)] AIT Austrian Institute of Technology, 1190 Vienna, Austria

[c)] Institute of Biology, University of Neuchâtel, 2000 Neuchâtel, Switzerland

[d)] Dept. of Agriculture, Food & Environment, University of Pisa, 56124 Pisa, Italy

[e)] Buesgen-Institute, Dept. of Forest Zoology and Forest Conservation, University of Göttingen, 37077 Göttingen, Germany

[f)] Institute of Chemical Technologies and Analytics, Vienna University of Technology, Getreidemarkt 9/164-UPA, 1060 Vienna, Austria.

‡ These authors contributed equally to this work

Corresponding author:
Tel.: +4350550-4002;
Fax: +4350550-4000
E-mail address: wolfgang.knoll@ait.ac.at

Highlights

- We made field effect transistors with graphene-immobilized odorant-binding proteins
- Such devices respond to odorants with trends similar to those of the native protein
- The biosensor is finely tuned to phenolic natural compounds, as the native protein
- Protein mutants have been also investigated using the same approach

Abstract

We describe the fabrication and performance of a biosensor for odorants, using wildtype and engineered mutants of the Italian honeybee (*Apis mellifera ligustica*) odorant binding protein 14 (OBP14), immobilized onto a reduced graphene oxide field-effect transistor (rGO-FET). The binding properties of the protein when immobilized on the biosensor are similar to those measured in solution, thus providing a method for measuring affinities to small molecules as an alternative to the current fluorescence assay. Out of the 14 chemicals tested, the best ligands for wildtype OBP14 were eugenol, homovanillic acid and related compounds sharing a phenol-methoxy backbone. Other chemicals, including methyl eugenol, showed affinities to OBP14 100-1000 times lower. We have also tested two mutants of OBP14. The first, bearing a HisTag at its N-terminus for better orientation on the sensor surface, showed only minor differences in its binding properties for chemicals when compared to the wildtype. The second contained an additional disulfide bond between helices α3 and α6, thus reducing the dynamics of OBP14 and leading to a higher affinity for eugenol. These data also demonstrate that it is feasible to produce biosensors with desired ligand specificities by introducing selected mutations into the structure of OBPs or other active proteins.

Keywords: honeybee (*Apis mellifera)*, odorant detection, odorant-binding protein, reduced graphene oxide, olfactory electronic biosensor, field-effect transistor

1. Introduction

Insects detect and discriminate olfactory cues with specialized sensilla, mainly located on the antennae, through the action of membrane-bound olfactory receptors [ORs; 1,2] and soluble odorant binding proteins (OBPs). The latter are small acidic polypeptides (~13-16 kDa) highly concentrated in the lymph of the chemosensilla [3-7]. Based on their ligand-binding properties, OBPs have been suggested to act as carriers for hydrophobic odorants and pheromones through the aqueous sensillar lymph to the odorant receptors, which are located in the membrane of olfactory neurons. Recently, however, evidence has been reported that OBPs might play additional roles assisting in the discrimination between different volatile organic compounds [8-14]. Moreover, functional studies with ORs expressed in heterologous systems provided evidence that the presence of the appropriate OBPs increases the sensitivity and selectivity of ORs to pheromones [15-18].

Thanks to recent genome and transcriptome projects, a high number of insect OBP sequences are available and three-dimensional structures have been solved for more than 20 of them [19-25]. In a few cases, as with OBP14 of the honeybee, ligands inside the hydrophobic cavity of the protein have been visualized by X-ray crystallography [24].

All OBPs share a common compact folding of six α-helical domains, further stabilized by three interlocked disulfide bridges in classic OBPs and two bridges in so-called “C-minus” OBPs, endowed with 4 or 5 cysteines [26,27]. As a consequence, the structure of OBPs is exceptionally stable to temperature, solvents and proteolysis [5,28,29]. These characteristics, combined with their simple and inexpensive production, make such proteins ideal and robust sensing elements for inclusion in artificial devices for environmental monitoring, medical diagnostics or food quality control [4].

A biosensor using an OBP or another binding protein would also offer an alternative label-free approach to measure binding affinities of odorant molecules. Currently, the most widely adopted method monitors the reduction in fluorescence [30-32], this approach needs a versatile fluorescent probe being capable to bind the protein and allowing to be competed by the odorant [5,33,34]. However, to validate the use of a biosensors for measuring binding constants, it is essential to demonstrate that the protein behaves similarly in solution and when immobilized on the sensing device.

In recent years, various biosensing devices mimicking the olfactory system have been developed [35-43] but only a limited series of studies using OBPs as target elements for the design of a 'bio-electronic nose' have been reported in the literature [44-48]. Following our first account, where we basically demonstrated the feasibility of the method [44], here we present the fabrication, operation, and quantitative characterization of a label-free biosensor for odorant detection based on reduced graphene oxide field-effect transistor (rGO-FET) functionalized with honeybee OBP14 as the active bio-mimetic sensing element [24,49]. Using our device, we have compared the specificity of the protein on the biosensor and in solution, and studied the responses of two OBP14 mutants, one featuring an additional disulfide bond, the second bearing an His-tag anchor for directional immobilization.

2. Materials and methods

2.1. Expression and purification of OBPs

Preparation of OBPs, selection of ligands, binding studies in solution and immobilization of OBPs on the rGO surface are described in the supplementary information.

2.2. Fabrication and electrical characterization of OBP-based biosensor devices

The whole assembly process follows our previously reported protocol [44] and was quantitatively examined using spectroscopic methods as described before [44]. The biosensor was established in a field effect transistor configuration with an Ag/AgCl liquid gate-, an Au source- and Au drain-electrode evaporated onto the functionalized surface (Fig.1, A). Reduced graphene oxide was contacted with electrodes and covered with OBP14 using the specific linker (Fig.1, B). Recordings of eugenol with the described biosensor device showed the specific current dependence on the gate voltage: In the source-drain current versus gate voltage (I_{SD}-vs-V_G) scans one can clearly distinguish between the two ambipolar branches typical of graphene FETs: the cathodic scan is dominated by the hole mobility, while the anodic scan is determined by the electron mobility, separated by the Dirac voltage seen at ca. V_G = 0.4 V. The used source-drain voltage was V_{SD} = 50 mV. Recording these I_{SD}-vs-V_G curves in aqueous solutions of ligands at different concentrations shows a distinct shift of the cathodic branch which we attribute to small variations of the electrical dipole of the OBP monolayer immobilized on the graphene gate surface upon the

binding of the ligands to the OBP. This significant concentration dependency appears for a range of gate voltages (cf. Fig.1C); for all kinetic and titration measurements (global analysis) the gate voltage was fixed to V_G = -0.6V. The electrical properties of such FET devices were tested as described before [44,50,51].

The general procedure for the entire kinetic/titration experiments started with continuously flushing the detection area with pure buffer (1 mM PBS, pH = 8.0) until a stable baseline of the source-drain current was established. Subsequently, the biosensor was titrated with different odorant concentrations in the range of 100 nM – 4 mM (depending on the ligand) and changes in source-drain current (ΔI_{DS}) were monitored in real time (cf. Fig. 2). A flow rate of 300 µL/min was chosen in order to minimize mass transfer of the analyte to the sensor surface [52-54]. Typically, a solution with a certain odorant concentration was injected into the measuring cell and the odorant was allowed to interact with the immobilized OBP14 until equilibrium was reached, as indicated by a constant source-drain current. This process was repeated with odorant solutions of different concentrations until saturation of the surface with the target analyte was reached and no significant further changes in the source-drain currents were detected. Surface titration experiments were terminated by a final washing with pure buffer in order to dissociate ligands from their complexes with OBP14, resulting in a typically complete restoration of the initial baseline current. In almost all devices, a very moderate drift of the source-drain current was observed with time. For this reason, the drain current response curves were normalized by subtraction of the (interpolated) baseline current. Kinetic and equilibrium parameters of the above described kinetic/titration experiments were globally analysed using the Langmuir model as described previously [44].

3. Results

3.1. Kinetic and titration experiments with WT-OBP14

We first assembled a rGO-FET sensor, functionalized with the *A. mellifera* WT-OBP14, and recorded its response to odorants applied in solution through the flow cell. As in our previous paper [44], we have decided to immobilize the sensing protein on a field-effect transistor (FET) on the basis that a three-terminal-device offers the possibility of determining a number of additional characterization parameters as compared to a simpler two-terminal-device (current measurements). Examples are electron and hole mobilities (μ_{el} and μ_h), respectively, the threshold voltage (V_{th}), the

transfer function and others [55,56]. We have studied these aspects theoretically and experimentally for rGO FETs and their use in various settings in biosensing [54]. Fig. 2 shows the results of a typical experiment. The variations in the source-drain current (I_{DS}) of a rGO-FET during exposure to eugenol solutions from 10 μM to 100 μM are recorded in real-time. Rinsing with pure buffer between ligand applications brings the current signal back to the baseline level, indicating the reversibility of the process. Since eugenol is a neutral compound, we propose that binding of this ligand modifies the dipole distribution within the odorant binding protein immobilized on the gate, coupling capacitively to the conductive channel of the transistor.

Most relevant for using this electronic device as a quantitative biosensor is the fact that the current change is related in a unique (and reproducible) way to the analyte occupancy of the binding pocket, which depends on its concentration in the bulk solution. The observation that the interaction is fully reversible is important, i.e. the analyte can be fully washed away by rinsing with buffer. This is a prerequisite for applying the Langmuir model for the quantitative analysis of the kinetic and thermodynamic equilibrium parameters of the system.

In a second experiment, we titrated OBP14 immobilized on the same sensor with homovanillic acid solutions in order to construct a full Langmuir binding curve. As in a similar experiment reported in our previous paper [44], the sensor response was measured by monitoring changes in the source-drain current (ΔI_{SD}), while higher amounts of the odorant were successively applied as aqueous solutions through the flow cell (Fig. 3A). At each concentration step we can observe a change of I_{SD} reaching a new stationary level. Plotting these values of the changes of the stationary currents, ΔI_{SD}, relative to their extrapolated maximum values, $\Delta I_{SD,max}$, i.e. $\Theta = \Delta I_{SD}/\Delta I_{SD,max}$, as a function of the applied concentration of homovanillic acid, produced a typical Langmuir binding isotherm (Fig. 3B). The data points can be well described by the equation:

$$\Theta = K_A c_{HV} / (K_A c_{HV} + 1) \qquad \text{Equation (1)}$$

with the affinity constant $K_A = 2.5\ 10^5\ M^{-1}$ (cf. red solid curve in Fig. 3B).

A closer inspection of the binding and dissociation events allows for the evaluation of the kinetic association and dissociation rate constants. Fig. 3C provides a detailed plot of the time dependent current change, ΔI_{SD}, from the steady state value reached

at 6 μM ligand concentration to the new stationary level reached after increasing the bulk odorant concentration to 10 μM with the solid line fit curve giving the corresponding rate constant.

By plotting all measured k-values as a function of the bulk concentration of homovanillic acid we obtain a linear increase in the rate constants k (Fig. 3E) as predicted by the Langmuir model:

$$k = k_{on}\, c_{HV} + k_{off} \qquad \text{Equation (2)}$$

from which we can determine the on rate, k_{on}, as the slope of the fit line, and k_{off} as the intersection with the y-axis.

As an internal consistency check, the dissociation process can also be observed as an increase of the source-drain current (back to the background current) upon switching the bulk odorant concentration to zero, i.e. rinsing again with pure buffer through the flow cell (Fig. 3D). According to the Langmuir model (cf. Eqn 2 with $c_{HV} = 0$), the corresponding data can be fitted by a single exponential curve indicating that the dissociation rate constant $k_{off} = 0.008\ s^{-1}$ and its error margins $0.0064\ s^{-1} < k_{off} < 0.0096\ s^{-1}$ are in good agreement with the extrapolated value from Fig. 3E.

According to the Langmuir model, the relation between the rate constants and the affinity constant is given by:

$$K_A = k_{on} / k_{off} \qquad \text{Equation (3)}$$

With the rate constants derived from fits to the data like those presented on Fig. 3E one obtains, according to Eqn. (3), a second set of affinity constants K_A (or their inverse, i.e., the dissociation constants, K_d) that can be compared with those derived from titration experiments (Fig. 3B). Fig. 4 reports both sets of values, i.e., $K_{d,LI}$ from the titration experiments (Langmuir isotherm plot) and $K_{d,kin}$ from the kinetic runs (k versus c plot). We see that for each ligand the difference between the two values is lower than a factor of 3. Given the fact that one measurement is from an equilibrium titration experiment while the other is from kinetic runs with different doses of ligand, this agreement is satisfactory and confirms the assumption that the binding of odorants to OBPs is fully reversible and can be described by the Langmuir model.

3.2. Specificity of OBP14-functionalized sensor

Using the electronic biosensor assembled with honeybee OBP14, we have measured the binding of some floral and pollen specific odorants, as well as structurally similar compounds. At the same time, all the necessary blanks and references have been included, whose results are reported in the supplementary information. We have used 14 ligands (Fig. 4), confirming and extending the results obtained in our previous work [44]. In particular, the data relative to the ligands homovanillic acid, citral, methyl eugenol and geraniol have been already reported in our previous paper [44], while the others are new. The crystallographic structure of OBP14 complexed with eugenol showed the importance of the hydroxyl group of the ligand, situated at the appropriate position to establish hydrogen bonds with the hydroxyl residue of Ser108 and the carbonyl group of Lys111 [24].

To further verify and confirm this fact, we have included among our ligands compounds in which the hydroxyl group is either conserved or masked (Fig. 4). The measured affinity constants, as reported in Fig. 4, are derived from the Langmuir isotherm ($K_{d,LI}$, cf. equation 1) as well as from the reaction rate constants, $K_{d,kin}$, for each of the tested ligands (cf. equation 2) and are reported in the order: equilibrium affinity constants (in bold), k_{on}, k_{off} and $K_{d,kin}$, derived from the measured reaction rate constants.

We can observe that:

1. our ligands display affinity constants across 3 orders of magnitude;
2. The affinity constants for ligands very similar in structure, e.g., eugenol and methyl eugenol, can vary by a factor of 35, indicating good selectivity of the sensor [44];
3. all good ligands for OBP14 (homovanillic acid, coniferyl aldehyde, vanillyl acetone, methyl vanillate, coniferyl alcohol, vanillin, eugenol) share a phenolic group as a common structural feature; masking such group, as in the molecule of methy leugenol results in a substantial loss of affinity;
4. all non aromatic structures proved to be non ligands for honeybee OBP14;
5. between strong and weak ligands the dissociation rate constants, k_{off}, vary by only a factor of three, while association rate constants, k_{on}, span nearly 3 orders of magnitude.

3.3. Binding of ligands to mutants of OBP14

Further, we performed experiments with two mutants of OBP14. The first one, HisTag-OBP14, contained an additional segment of six histidines at its N-terminus. This modification was introduced with the aim of immobilizing the protein on the sensor surface in an oriented fashion, using a bifunctional pyrene-NTA-linker. As this mutant had not been described before, we measured its binding to the fluorescent probe N-phenyl-1-aminonaphthalene (1-NPN) in solution (cf. also Fig. S4) and found a lower affinity (K_d = 2.9 μM) compared to the wild type protein (K_d = 0.32 μM, cf. the solution binding data presented in Fig. S2) [24].

The second mutant (S-S-OBP14) contains two additional cysteines, joined in a third disulphide bond, to reproduce the six-cysteine motive of classical OBPs and confer better stability to the protein [24,29].

Fig. 5 reports the results of binding experiments of eugenol to WT-OBP14 and its two mutants immobilized on the sensor. The affinity of this ligand to the wild-type OBP14 was measured in our previous work [44]. Here, while we verified a good reproducibility of the results with the WT, we investigate the effect of mutations on the binding of this good ligand. In particular, we can observe that:

1. the oriented immobilization of the HisTag-OBP14 did not generate a higher current signal, nor did it significantly modify the rate constants; instead, it produced a signal with a lower intensity when compared to the wild type protein immobilized through random links (Fig. 5 A and B). This effect could be due to an increased distance of the protein from the surface of the sensor when using the relatively long NTA spacer, thus reducing the capacitive coupling of the dipole changes produced by ligand binding to the rGO-FET measuring channel (Fig. 1B);
2. the HisTag-OBP14 mutant shows only little differences in rate constants and affinity constants compared to the WT-OBP14 (cf. Table 1). This fact was observed with eugenol, isoamyl acetate and geraniol, representative of strong, medium and weak ligands, respectively (Table 1);
3. in the double mutant (S-S-OBP14: Gln44Cys, His97Cys), the introduction of a third disulphide bridge strongly affects the binding properties of the protein (Fig. 5C). This can be seen in the shift of the Langmuir isotherm in Fig. 5D, as well as in the slope of the rate constants in Fig. 5E (cf. also the values for k_{on}, k_{off}, and K_d, given in Table 1). The increase in the binding strength by a factor

of 10 relative to the wild type is quite significant, and offers the possibility of modifying the binding properties of OBPs by site-directed mutagenesis.

4. Discussion

4.1. Affinity constants for ligands with a basic phenolic structure

Using the honeybee OBP14 as sensing element, we have assembled an electronic device narrowly tuned to odorants containing phenolic structures. The presence of a free hydroxyl group in para position is essential for good affinity of the ligand to the protein. This group establishes a specific hydrogen bond with the carbonyl of Lys 111, as shown in the crystal structure of OBP14 complexed with eugenol [24].

In a previous study using circular dichroism we had shown that ligands bound to OBP14 increase the thermal stability of the protein [29] (cf. Fig. S4). We had further demonstrated that the increase in thermal stability correlated with the binding strength of the ligand, being highest for phenolic compounds.

Besides confirming such a structural specificity, the study presented here provides further support to the fact that the hydroxyl group is specifically essential for good fitting of the ligand to the protein, both in the biological system and in the rGO-FET device. In fact, homovanillic acid and coniferyl aldehyde, both endowed with a free hydroxyl group, proved to be the strongest ligands investigated. On the other hand, while eugenol is a strong ligand, its close derivative, methyl eugenol showed much poorer affinity. Moreover, we find another substitution pattern dependence that plays a major role in ligand recognition: Comparison of the two phenolic compounds, eugenol and homovanilic acid, which differ in terms of a carboxyl / ethenyl substitution, shows a ~6 fold difference of affinities (Table 1). In addition, the obtained affinity constants from the non-aromatic small molecules, showed much lower affinities (as the ligands citral, geraniol, isoamyl acetate and sulcatone). These phenylpropenes play an important role in plant pollination by bees and in the chemical ecology of fruit flies [57]. In terms of sensitivity, we have shown that a variation of 4 μM in the concentration of the analyte (Fig. 3C) produces a signal that is clearly detected and measured with a high degree of confidence, indicating that our sensor can be used in situations where micro-molar accuracy is required.

4.2. Tuning ligand affinities by genetic manipulation of OBPs

The selectivity of OBP14 can be improved and in general modified by introducing structural modifications in the protein. In this study we have used, in addition to the wild type OBP14, a mutant bearing two amino acid substitutions with the consequent establishment of a third disulfide bridge (S-S-OBP14). This modification made the protein more rigid and increased its affinity to eugenol from 40 μM for the WT-OBP14 to 4 μM for the S-S-OBP14 mutant. The increase in thermal stability of the OBP14-eugenol complex was also higher for the mutant as compared to the wild type (Fig. S4).

These results represent a first step towards the design of new biosensors tailored to specific odorant molecules, which can be obtained by selective amino acid substitutions in the binding pockets of OBPs.

The introduction of a His-tag at the N-terminus of the protein, instead, did not improve the performance of the sensor, most likely because of the increased distance between the core of the protein and the graphene surface. However, such an approach, that allows regular alignment of the protein molecules on the sensor surface, should be further investigated using shorter polypeptide arms or different ways of immobilization.

Electronic devices, using an array of such biosensors, could eventually be applied to the analysis of complex mixtures of odorants, as those present in nature, with a strategy borrowed from the functioning of biological olfactory systems.

5. Conclusions

We have developed an olfactory biosensor based on a rGO-FET derivatised with OBP14 from the honeybee as the sensing element. Our device responds to several floral and pollen odorants with a sensitivity and selectivity matching those reported in fluorescent binding assays.

On the basis of these results, our biosensor can be used for directly measuring affinities of small ligand to a binding protein. Currently, by far the most adopted method for monitoring binding to a protein is based on the displacement of a fluorescent reporter, whose emission spectrum is modified when bound to the hydrophobic pocket of a protein [30]. Such an approach, although simple and rapid, requires a fluorescent compound with good affinity for the protein of interest. The biosensor here described, instead, can measure affinities without the need of a reporter molecule, nor does it require the use of radioactive ligands. Moreover, our

device, unlike other current techniques, allows measurement of kinetic parameters in addition to thermodynamic equilibrium constants.

Within a longer perspective, the results obtained with the two mutants of the protein create a basis for designing new biosensing elements with desired specificity, using site-directed mutagenesis to modify the scaffolding of the polypeptide chain, as well as the micro-environment of the binding pocket. Such strategies will represent a first step towards the development of arrays of biosensors with complementary specificities necessary to mimic the complexity and the sophisticated performance of an insect antenna or a vertebrate nose.

Acknowledgements

Partial support for this work was provided by the European Science Foundation (ESF), Grant Number 10-EuroBioSAS-FP-005, the Austrian Science Fund (FWF) (I681-N24), the Austrian Federal Ministry for Transportation, Innovation and Technology (GZ BMVIT-612.166/0001-III/I1/2010), by the FFG within the Comet program, from the governments of Lower and Upper Austria, and by the Swiss National Foundation, Grant Number 31BI30_134410/1 (NANOIOBIP).

References

1 Clyne PJ, Certel SJ, de Bruyne M, Zaslavsky L, Johnson WA, Carlson JR.The Odor Specificities of a Subset of Olfactory Receptor Neurons Are Governed by Acj6, a POU-Domain Transcription Factor. Neuron 1999; 22(2): 339-347.

2 Vosshall LB, Amrein H, Morozov PS, Rzhetsky A, Axel R. Molecular Architecture of Smell and Taste in Drosophila. Cell 1999; 96(5): 725-736.

3 Leal WS.Odorant reception in insects: roles of receptors, binding proteins, and degrading enzymes. Annu Rev Entomol 2013; 58(1): 373-391.

4 Pelosi P, Iovinella I, Felicioli A, Dani FR. Soluble proteins of chemical communication: an overview across arthropods. Front Physiol 2014; 5: 320

5 Pelosi P, Zhou JJ, Ban LP, Calvello M. Soluble proteins in insect chemical communication. Cell Mol Life Sci 2006; 63(14): 1658-1676.

6 Vogt RG. 2005. Molecular basis of pheromone detection in insects, in: Gilbert, L., Latro, K., Gill, S. (Eds.), Comprehensive Insect Physiology, Biochemistry, Pharmacology and Molecular Biology, Elsvier, London, pp. 753-804.
7 Vogt RG, Riddiford LM. Pheromone binding and inactivation by moth antennae. Nature 1981; 293(5828): 161-163.
8 Matsuo T. Odorant-binding proteins and evolution of host-plant preference in insects. Tanpakushitsu Kakusan Koso 2007; 52(15): 1980-1986.
9 Sun YF, De Biasio F, Qiao HL, Iovinella I, Yang SX, Ling Y, Riviello L, Battaglia D, Falabella P, Yang XL, Pelosi P. Two odorant-binding proteins mediate the behavioural response of aphids to the alarm pheromone (E)-ß-farnesene and structural analogues. PLOS One 2012; 7(3): e32759.
10 Swarup S, Williams TI, Anholt RR. Functional dissection of Odorant binding protein genes in Drosophila melanogaster. Genes Brain Behav 2011; 10(6): 648-657.
11 Xu P, Atkinson R, Jones DN, Smith DP. Drosophila OBP LUSH is required for activity of pheromone-sensitive neurons. Neuron 2005.;45(2): 193-200.
12 Qiao H, Tuccori E, He X, Gazzano A, Field L, Zhou JJ, Pelosi P. Discrimination of alarm pheromone (E)-β-farnesene by aphid odorant-binding proteins. Insect Biochem Mol Biol 2009; 39(5): 414-419.
13 Pelletier J, Guidolin A, Syed Z, Cornel AJ, Leal WS. Knockdown of a mosquito odorant-binding protein involved in the sensitive detection of oviposition attractants. J Chem Ecol 2010; 36(3): 245-248.
14 Biessmann H, Andronopoulou E, Biessmann MR, Douris V, Dimitratos SD, Eliopoulos E, Guerin PM, Iatrou K, Justice RW, Kröber T, Marinotti O, Tsitoura P, Woods DF, Walter MF. The Anopheles gambiae odorant binding protein 1 (AgamOBP1) mediates indole recognition in the antennae of female mosquitoes. PLOS ONE 2010; 5(3): e9471.
15 Grosse-Wilde E, Svatos A, Krieger J. A pheromone-binding protein mediates the bombykol-induced activation of a pheromone receptor in vitro. Chem Senses 2006; 31(6): 547–555.
16 Forstner M, Breer H, Krieger J.A receptor and binding protein interplay in the detection of a distinct pheromone component in the silkmoth Antheraea polyphemus. Int J Biol Sci 2009; 5(7): 745-757.
17 Sun M, Liu Y, Walker WB, Liu C, Lin K, Gu S, Zhang Y, Zhou J, Wang G.Identification and Characterization of Pheromone Receptors and Interplay between

Receptors and Pheromone Binding Proteins in the Diamondback Moth, Plutella xyllostella. PLOS ONE 2013; 8(4): e62098.
18 Chang H, Liu Y, Yang T, Pelosi P, Dong S, Wang G. Pheromone binding proteins enhance the sensitivity of olfactory receptors to sex pheromones in Chilo suppressalis. Sci Rep 2015; 5:13093.
19 Horst R, Damberger F, Luginbuhl P, Guntert P, Peng G, Nikonova L, Leal WS, Wuthrich K, NMR structure reveals intramolecular regulation mechanism for pheromone binding and release. Proc Natl Acad Sci USA 2001; 98(25): 14374-14379.
20 Kruse, SW, Zhao R, Smith DP, Jones DNM. Structure of a specific alcohol-binding site defined by the odorant binding protein LUSH from Drosophila melanogaster. Nat Struct Mol Biol 2003; 10(9): 694-700.
21 Lagarde A, Spinelli S, Tegoni M, He X, Field L, Zhou JJ, Cambillau C. The Crystal Structure of Odorant Binding Protein 7 from Anopheles gambiae Exhibits an Outstanding Adaptability of Its Binding Site. J of Mol Biol 2011; 414(3): 401-412.
22 Lescop E, Briand Lc, Pernollet JC, Guittet E. Structural Basis of the Broad Specificity of a General Odorant-Binding Protein from Honeybee. Biochemistry 2009; 48(11): 2431-2441.
23 Sandler BH, Nikonova L, Leal WS, Clardy J. Sexual attraction in the silkworm moth: structure of the pheromone-binding-protein–bombykol complex. Chem Biol 2000; 7(2): 143-151.
24 Spinelli S, Lagarde A, Iovinella I, Legrand P, Tegoni M, Pelosi P, Cambillau C. Crystal structure of Apis mellifera OBP14, a C-minus odorant-binding protein, and its complexes with odorant molecules. Insect Biochem Mol Biol 2012; 42(1): 41-50.
25 Wogulis M, Morgan T, Ishida Y, Leal, WS, Wilson DK. The crystal structure of an odorant binding protein from Anopheles gambiae: Evidence for a common ligand release mechanism. Biochem Biophys Res Commun 2006; 339(1): 157-164.
26 Leal WS, Nikonova L, Peng GH. Disulfide structure of the pheromone binding protein from the silkworm moth, Bombyx mori. FEBS Lett 1999; 464(1-2): 85-90.
27 Scaloni A, Monti M, Angeli S, Pelosi P. Structural analysis and disulfide-bridge pairing of two odorant-binding proteins from Bombyx mori. Biochem Biophys Res Commun 1999; 266(2): 386-391.

28 Calvello M, Guerra N, Brandazza A, D'Ambrosio C, Scaloni A, Dani FR, Turillazzi S, Pelosi P. Soluble proteins of chemical communication in the social wasp Polistes dominulus. Cell and Mol Life Sci 2003; 60(9): 1933-1943.
29 Schwaighofer A, Kotlowski C, Araman C, Chu N. Mastrogiacomo R, Becker C, Pelosi P, Knoll W, Larisika M, Nowak C. Insights into structural features determining odorant affinities to honey bee odorant binding protein 14. Eur Biophys J 2014; 43(2-3): 105-112.
30 Ban LP, Zhang L, Yan YH, Pelosi P. Binding properties of a locust's chemosensory protein. Biochem and Biophys Res Commun 2002; 293(1): 50-54.
31 Ban L, Scaloni A, Brandazza A, Angeli S, Zhang L, Yan Y, Pelosi P. Chemosensory proteins of Locusta migratoria. Insect Mol Biol 2003; 12(2): 125-134.
32 Campanacci V, Krieger J, Bette S, Sturgis JN, Lartigue A, Cambillau C, Breer H, Tegoni M. Revisiting the specificity of mamestra brassicaeand Antheraea polyphemus pheromone-binding proteins with a fluorescence binding assay. J Biol Chem 2001; 276(23): 20078-20084.
33 Mastrogiacomo R, Iovinella I & Napolitano E. New fluorescent probes for ligand-binding assays of odorant-binding proteins. Biochem Biophys Res Commun 2014; 446(1): 137-142.
34 Fan J, Francis F, Liu Y, Chen JL, Cheng DF. An overview of odorant-binding protein functions in insect peripheral olfactory reception. Genet Mol Res 2011; 10(4): 3056-3069.
35 Hou Y, Jaffrezic-Renault N, Martelet C, Zhang A, Minic-Vidic J, Gorojankina T, Persuy MA, Pajot-Augy E, Salesse R, Akimov V, Reggiani L, Pennetta C, Alfinito E, Ruiz O, Gomila G, Samitier J, Errachid A. A novel detection strategy for odorant molecules based on controlled bioengineering of rat olfactory receptor I7. Biosens and Bioelectron 2007; 22(7): 1550-1555.
36 Jin HJ, Lee SH, Kim TH, Park J, Song HS, Park TH, Hong S. Nanovesicle-based bioelectronic nose platform mimicking human olfactory signal transduction. Biosens and Bioelectron; 2012: 35(1), 335-341.
37 Kim TH, Lee SH, Lee J, Song HS, Oh EH, Park TH, Hong S. Single-Carbon-Atomic-Resolution Detection of Odorant Molecules using a Human Olfactory Receptor-based Bioelectronic Nose. Adv Mater 2009; 21(1): 91-94.

38 Lee SH, Jin HJ, Song HS, Hong S, Park TH. Bioelectronic nose with high sensitivity and selectivity using chemically functionalized carbon nanotube combined with human olfactory receptor. J Biotechnol 2012; 157(4): 467-472.
39 Lee SH, Jun SB, Ko HJ, Kim SJ, Park TH. Cell-based olfactory biosensor using microfabricated planar electrode. Biosens and Bioelectron 2009; 24(8): 2659-2664.
40 Liu Q, Wang H, Li H, Zhang J, Zhuang S, Zhang F, Jimmy Hsia K, Wang P. Impedance sensing and molecular modeling of an olfactory biosensor based on chemosensory proteins of honeybee. Biosens and Bioelectron 2013; 40(1): 174-179.
41 Park J, Lim JH, Jin HJ, Namgung S, Lee SH, Park TH, Hong S. A bioelectronic sensor based on canine olfactory nanovesicle–carbon nanotube hybrid structures for the fast assessment of food quality. Analyst 2012; 137(14): 3249-3254.
42 Park SJ, Kwon OS, Lee SH, Song HS, Park TH, Jang J. Ultrasensitive flexible graphene based field-effect transistor (FET)-type bioelectronic nose. Nano Lett 2012; 12(10): 5082-5090.
43 Yoon H, Lee SH, Kwon OS, Song HS, Oh EH, Park TH, Jang J. Polypyrrole Nanotubes Conjugated with Human Olfactory Receptors: High-Performance Transducers for FET-Type Bioelectronic Noses. Angew Chem Intern Ed 2009; 48(15): 2755-2758.
44 Larisika M, Kotlowski C, Steininger C, Mastrogiacomo R, Pelosi P, Schütz S, Peteu SF, Kleber C, Reiner-Rozman C, Nowak C, Knoll W. Electronic Olfactory Sensor Based on *A. mellifera* Odorant-Binding Protein 14 on a Reduced Graphene Oxide Field-Effect Transistor. Angew Chem Int Ed 2015; 54: 13245-13248.

45 Mulla MY, Tuccori E, Magliulo M, Lattanzi G, Palazzo G, Persaud K, Torsi L. Capacitance-modulated transistor detects odorant binding protein chiral interactions. Nat Commun; 2015: 6.
46 S. D_Auria S, Scognamiglio V, Rossi M, Staiano M, Campopiano N, Cennamo S, Zeni L. In: Conference on Biomedical Vibrational Spectroscopy and Biohazard Detection Technologies, Vol. 5321, SPIE—The International Society for Optical Engineering, San Jose California (USA), 2004, p. 258.
47 Di Pietrantonio F, Cannatà D, Benetti M, Verona E, Varriale A, Staiano M, D'Auria S. Detection of odorant molecules via surface acoustic wave biosensor array based on odorant-binding proteins. Biosens and Bioelectron 2013; 41(0): 328-334.

48 Sankaran S, Panigrahi S, Mallik S. Odorant binding protein based biomimetic sensors for detection of alcohols associated with Salmonella contamination in packaged beef. Biosens Bioelectron 2011; 26(7): 3103-3109.
49 Iovinella I, Dani FR, Niccolini A, Sagona S, Michelucci E, Gazzano A, Turillazzi S, Felicioli A, Pelosi P. Differential Expression of Odorant-Binding Proteins in the Mandibular Glands of the Honey Bee According to Caste and Age. J Proteome Res 2011; 10(8): 3439-3449.
50 Huang J, Larisika M, Fam DWH, He Q, Nimmo MA, Nowak C, Tok AIY. The extended growth of graphene oxide flakes using ethanol CVD. Nanoscale 2013; 5(7): 2945-2951.
51 Reiner-Rozman C, Larisika M, Nowak C, Knoll W. Graphene-based liquid-gated field effect transistor for biosensing: Theory and experiments. Biosens Bioelectron 2014; 70: 21-27.
52 Adamczyk M, Moore JA, Yu ZG. Application of surface plasmon resonance toward studies of low-molecular-weight antigen-antibody binding interactions. Methods-a Companion to Methods in Enzymology 2000; 20(3): 319-328.
53 Karlsson R, Falt A. Experimental design for kinetic analysis of protein-protein interactions with surface plasmon resonance biosensors. J Immunol Methods 1997; 200(1-2): 121-133.
54 Khan HU, Jang J, Kim JJ, Knoll W. In Situ Antibody Detection and Charge Discrimination Using Aqueous Stable Pentacene Transistor Biosensors. J Am Chem Soc 2011; 133(7): 2170-2176.
55 Mao S, & Chen J. Graphene-based electronic biosensors. J Mater Res 2017; 1-12.
56 Andronescu C, Schuhmann W. Graphene-based Field Effect Transistors as Biosensors. Curr Opin Electrochem 2017.
57 Metcalf RL. Chemical Ecology of Dacinae Fruit Flies (Diptera: Tephritidae). Ann Entomol Soc Am 1990; 83 (6): 1017-1030.

Caroline Kotlowski received her MSc in Chemical Engineering from the Vienna University of Technology (Austria) with the major field of study on Bioanalytics and Biotechnology and her PhD in Nanobiotechnology from the University of Natural Resources and Life Sciences, Vienna (Austria). Her work is focused on the chemical recognition on sp^2 carbon surfaces by developing field-effect transistor based sensing platforms.

Melanie Larisika studied Biology at the Johannes Gutenberg University Mainz and finished 2010 with a PhD thesis at the Institute of Microbiology and Wine Research. She spend a year as a postdoc at the Nanyang Technological University in Singapore before joining the Biosensor Technologies group at the AIT Austrian Institute of Technology working on electronic smell sensing.

Patrick Guerin received his PhD from University College Dublin and worked on insect plant relations for the first15 years of his career. In 1987 he took up a position as Director of Research at the Faculty of Science, University of Neuchâtel, Switzerland where he has worked on the sensory physiology and behaviour of ticks and insect vectors of disease.

Christoph Kleber studied Physical and Theoretical Chemistry, earned his PhD degree in Analytical Chemistry from the Technical University Vienna and did his "Habilitation in Material Science". From 2002-2008 he was Professor at the University of Applied Sciences in Krems, from 2008-2010 Manager in the Air Liquide Group and since 2010 he is the Scientific Director of the Centre of Excellence for Electrochemical Surface Technology and since 2016 he is visiting professor at the Institute for Chemical Technologies of Inorganic Materials (Prof. Hassel) at the Johannes Kepler University Linz.

Thomas Kroeber is a senior researcher working on the sensory physiology and behaviour of insect vectors of disease at the Biology Institute, University of Neuchâtel, Switzerland, where he completed his PhD in 2000. He is interested in applied research pertaining to olfaction, taste and thermoreception in arthropods. He participated in this biosensor project as he is fascinated by the prospect of using sensory proteins of insects to build sensitive biosensors.

Rosa Mastrogiacomo graduated from the University of Pisa, Italy and received a PhD in Neuroscience from the University of Genova, Italy. After graduation, she worked on odorant-binding proteins within the project EuroBioSAS at University of Pisa. Currently she is post-doc at Italian Institute of Technology, Genova, working in the Genetic of Cognition lab with Dr. Papaleo.

Christoph Nowak finished 2010 his education in Chemistry at the Johannes Gutenberg University of Mainz with a PhD dissertation entitled “Infrared Spectroscopy on Redox Membrane Proteins in a Biomimetic Membrane Architecture”. After a postdoctoral stay at the Nanyang Technological University in Singapore where he started a project on the design of rGO- based field - effect transistors, he joined in 2011 the AIT Austrian Institute of Technology as a group leader for electronic smell sensing.

Paolo Pelosi is retired professor from the University of Pisa, currently visiting professor at the Chinese Academy of Agricultural Sciences, Beijing, China. His research has been focused on chemical and biochemical aspect of olfaction, with particular reference to odorant-binding proteins.

Stefan Schütz is the head of the department of Forest Zoology and Forest Protection, at the University of Göttingen. His main interests are in the fields of Chemical Ecology of plant-fungus-insect interaction, the relation between semiochemical diversity, biodiversity, and ecosystem functions, and the design of biosensors and biomimetic sensor systems.

Andreas Schwaighofer is a postdoctoral researcher at the Institute of Chemical Technology and Analytics at TU Wien, Austria. He received his PhD at the University of Natural Resources and Life Sciences, Vienna, Austria. His work focuses on applying spectroscopic methods to study the stability and structural changes of proteins upon external perturbation,

ligand binding and denaturation. Currently, his research interests include QCL-IR transmission measurements in aqueous solution for secondary structure analysis of proteins.

Wolfgang Knoll earned a PhD degree in Biophysics from the University of Konstanz in 1976 and the "Habilitation in Experimental Physics" in 1986 from the Technical University of Munich. From 1991-1999 he was the Laboratory Director for Exotic Nanomaterials in Wako, Japan, at the Institute of Physical and Chemical Research (RIKEN), and from 1993 to 2008, Director at the Max Planck Institute for Polymer Research in Mainz, Germany. Since 2008 he is the Scientific Managing Director of the AIT Austrian Institute of Technology.

Figure legends

Fig. 1. (A) Scheme of the set-up and device configuration consisting of an Ag/AgCl liquid gate electrode, an Au source- and Au drain-electrode, evaporated onto reduced graphene oxide flakes which were deposited onto the silicon substrate and functionalized with OBPs. The artist's sketch shows the functionalization with OBPs (lower right of A). The assembled flow cell with the sensor, inlet and outlet for odorants is given lower left inset of A; (B) fabrication and functionalization of rGO-FETs onto a silicon wafer with 300 nm SiO_2 and reduced graphene oxide (rGO) flakes with subsequent approach placing source and drain electrodes (5 nm Cr and 70 nm Au), followed by the 1-pyrenebutanoic acid succinimidyl ester (PBSE)-linker, (or NTA-linker), coupling the OBP14 to the surface (cf. suppl. inf.), followed by protein (OBP14) immobilization; (C) current versus voltage, (I_{SD}-vs-V_G), recordings of the OBP14 functionalized FET-biosensor at detecting different eugenol concentrations (indicated with different colors) flowing through the cell.

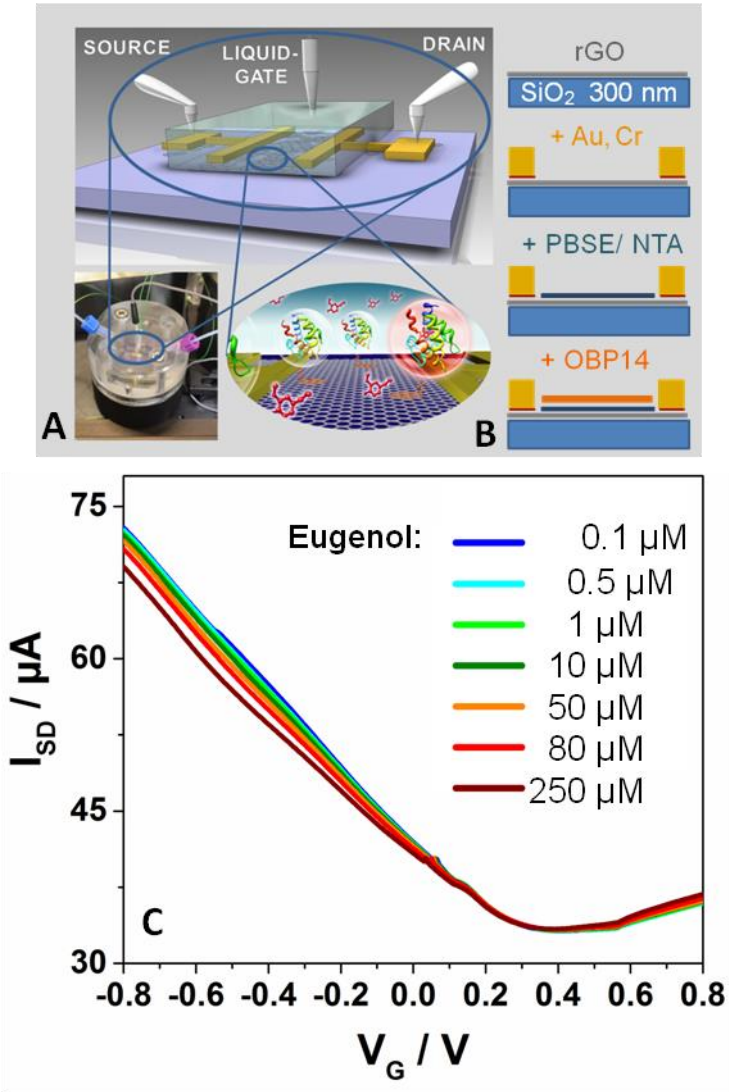

Fig. 2. On-line time recording and global measurements (kinetic and titration). The source-drain-current, I_{DS}, was monitored (black line) upon addition of odorant molecules (eugenol in this case, cf. inset) at different concentrations to the buffer (red arrows pointing up with correspondent concentration values), which flow across the gate of the rGO field-effect-transistor in the flow cell, changes the I_{SD}.Rinsing with pure buffer between stimulus applications (blue arrows pointing down) brings the current signal back to the baseline level, indicating the reversibility of the process.

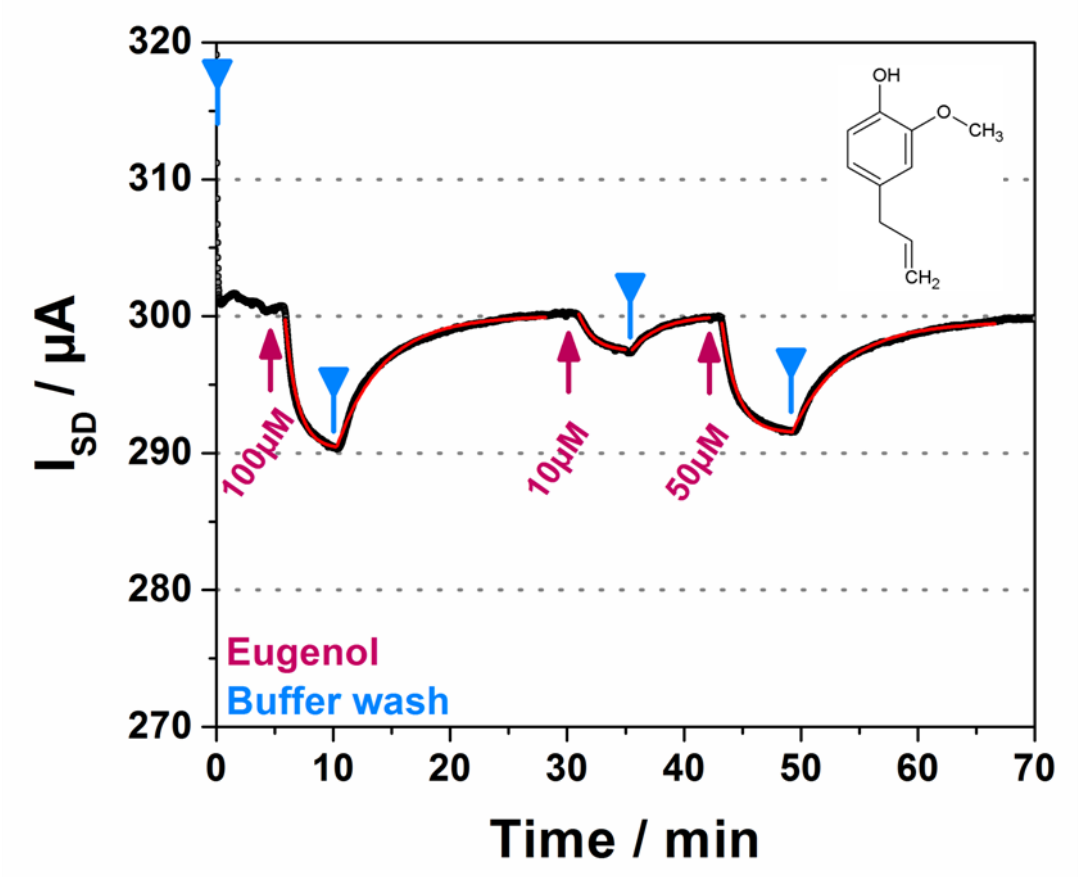

Fig. 3. Full analysis of the binding of homovanillic acid to OBP14: (A) global analysis for homovanillic acid binding to WT-OPB14 on the FET gate surface; different concentrations of homovanillic acid (indicated with red arrows pointing up, the correspondent concentration values in µM); buffer wash at the beginning and end of the measurement (indicated with blue arrows pointing down). (B) Langmuir binding isotherm diagram given by the data from panel (A): ΔI_{SD} of each tested concentration (circles) and the red solid a fitting curve with error margins in red (K_A+20% , K_A=3.0 10^5 M^{-1} (dash-dotted line), and (K_A -20%, K_A=2.0 10^5 M^{-1} (dotted line). (C) determination of the rate constant k and its error margins for one concentration, exemplified for the monitored real-time current change, ΔI_{SD}, after injection of 10 µM odorant solution: reaction rate constant k being the fit (red solid line) of the data points (black) k=0.024 s^{-1}, , and corresponding error margins dash-dotted line with k'= k + 20%, and dotted line, k''= k - 20%; (D) determination of the rate constant k_{off} : being the fit (red solid line) ofthe experimental data, ΔI_{SD}, after flushing the gate surface with buffer (arrow), k=0.008 s^{-1}, and corresponding error margins: dash-dotted line with k'= k + 20%, and dotted line with k''= k - 20%; (E) evaluation of the rate constants (k_{on}, k_{off}) given the linear fit (red line) of the reaction rate constants fits of each concentration step(circles), reaction rate constants are derived as exemplary

explained in panelin (C), are plotted as a function of the bulk concentration, c_{HV} , and k_{on}, k_{off} given by equation 2: k_{on} = 1130 $M^{-1}s^{-1}$ being the slope, and the intersection of the fit line with the ordinate, i.e. k for c_{HV} = 0, yields k_{off} = 0.008 s^{-1}.

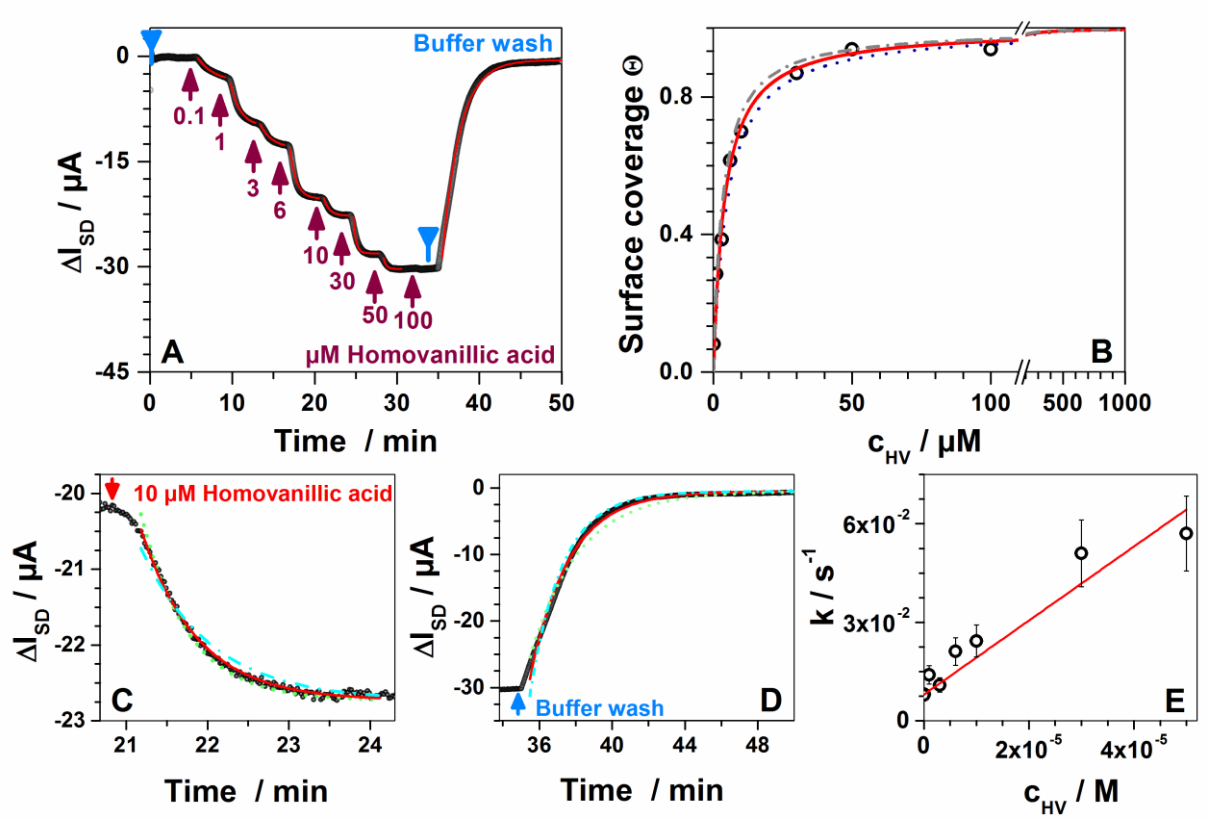

Fig. 4. Binding affinities of the odorants tested. The values reported are in the order: equilibrium affinity constants ($K_{d,\ LI}$, in bold), k_{on}, k_{off} and $K_{d,\ kin}$, derived from the measured reaction rate constants. All ligands share a phenol group, such as in eugenol and structurally related compounds, that proved essential for a good affinity, as shown by the lack of binding of methyl eugenol. All non aromatic structures proved not to be ligands for honeybee OBP14.

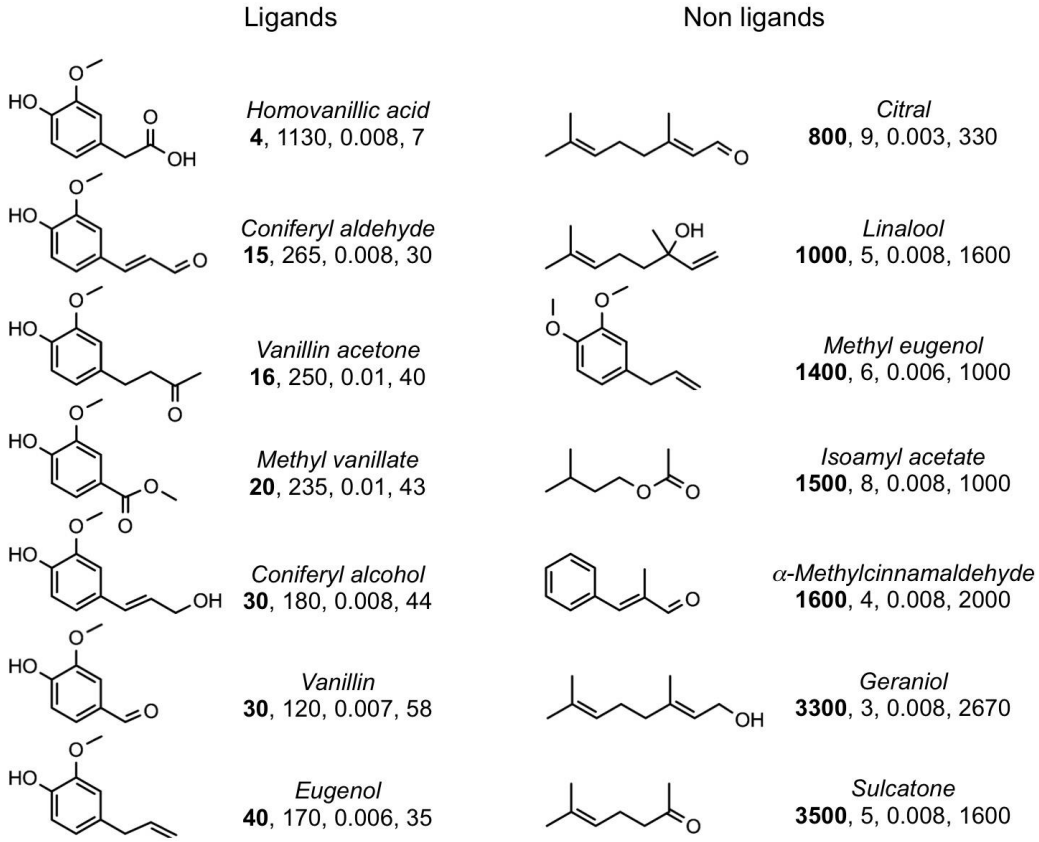

Fig. 5. Full analysis of binding of the odorant eugenol to the three odorant binding proteins: (A), WT-OBP14, (B), HisTag-OBP14, (C), S-S-OBP14. Panels A-C show the global analysis, different concentrations of eugenol (indicated with red arrows pointing up, the correspondent concentration values in µM); and buffer wash at the beginning, as well as at the end of the measurement (indicated with blue arrows pointing down). The red solid curves represent fits to the data(black line) . (D) Langmuir isotherms of eugenol binding to the three odorant binding proteinsgiven by the data in panels (A-C): ΔI_{SD} of each tested concentration: WT-OBP14 (circles), HisTag-OBP14 (squares), S-S-OBP14 (triangles) is shown . T, the red sigmoidal fitting curves with error margins: affinity constants, K_d, error margins K_d +20% (dash-dotted line), and K_d -20% (dotted line). Affinity constants K_d are as summarized in table 1. (E) Evaluation of the rate constants (k_{on}, k_{off}) given the linear fit (red line) of the reaction rate constants of each concentration step C, WT-OBP14 (circles), HisTag-OBP14 (squares), S-S-OBP14 (triangles), reaction rate constants are derived as explained in Fig.3,with +/- 20% error margins, . and are plotted as a function of the bulk concentration, c_{HV}, and k_{on}, k_{off} given by equation 2: k_{on} being the slope, and the intersection of the fit line with the ordinate, i.e. k for $c_{HV} = 0$, yields k_{off}.

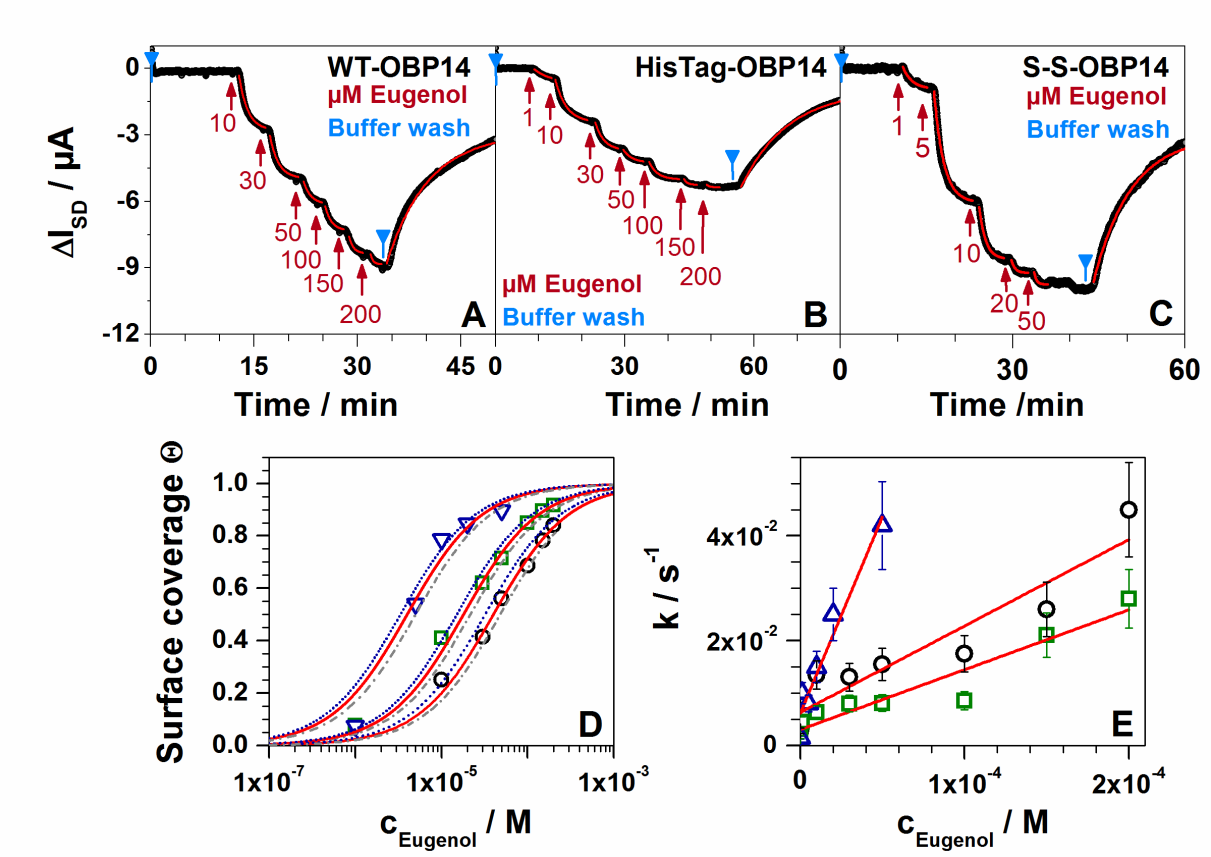

Table 1. Association rate constants, k_{on}, dissociation rate constants, k_{off}, and dissociation constants, K_d, for the three OBPs, WT-OBP14, HisTag-OBP14, and S-S-OBP14, tested with eugenol, isoamyl acetate, and geraniol.

WT - OBP14	k_{on} / $M^{-1}s^{-1}$	k_{off} / s^{-1}	K_d / µM
Eugenol	160	0.006	40
Isoamyl acetate	8	0.008	1000
Geraniol	2.5	0.008	3200
HisTag - OBP14	k_{on} / $M^{-1}s^{-1}$	k_{off} / s^{-1}	K_d / µM
Eugenol	110	0,003	20
Isoamyl acetate	6	0.009	1000
Geraniol	2	0.006	3700
S-S - OBP14	k_{on} / $M^{-1}s^{-1}$	k_{off} / s^{-1}	K_d / µM
Eugenol	750	0.006	4